Effects of curvature radius on vulnerability of curved bridges subjected to near and far-field strong ground motions

Ali Naseri[*1], Alireza MirzaGoltabar Roshan[2a],
Hossein Pahlavan[3b] and Gholamreza Ghodrati Amiri[4c]

[1]*Structural Engineering, Babol Noshirvani University of Technology, Iran*
[2]*Babol Noshirvani University of Technology, Iran*
[3]*Earthquake Engineering, Shahrood University of Technology, Iran*
[4]*Center of Excellence for Fundamental Studies in Structural Engineering, Univ. of Science and Technology, School of Civil Engineering, Iran*

Abstract. The specific characteristics of near-field earthquake records can lead to different dynamic responses of bridges compared to far-field records. However, the effect of near-field strong ground motion has often been neglected in the seismic performance assessment of the bridges. Furthermore, damage to horizontally curved multi-frame RC box-girder bridges in the past earthquakes has intensified the potential of seismic vulnerability of these structures due to their distinctive dynamic behavior. Based on the nonlinear time history analyses in OpenSEES, this article, assesses the effects of near-field versus far-field earthquakes on the seismic performance of horizontally curved multi-frame RC box-girder bridges by accounting the vertical component of the earthquake records. Analytical seismic fragility curves have been derived thru considering uncertainties in the earthquake records, material and geometric properties of bridges. The findings indicate that near-field effects reasonably increase the seismic vulnerability in this bridge sub-class. The results pave the way for future regional risk assessments regarding the importance of either including or excluding near-field effects on the seismic performance of horizontally curved bridges.

Keywords: curvature radius; curved bridges; seismic fragility; near and far-field; probabilistic vulnerability; damage monitoring system

1. Introduction

Earthquake, as one the most important natural phenomenon, occasionally causes economic losses to structures and fatalities in many countries. The deterioration of road bridges, which act as the main and vital structures constructed on the essential municipal artery, can deliver adverse consequences during the seismic events. Undoubtedly, the collapse of a bridge can severely jeopardize the pedestrians and vehicles in the vicinity, necessitating the significance of rehabilitation

∗Corresponding author, Ph.D., E-mail: Alinaseri@stu.nit.ac.ir
[a] Ph.D., E-mail: ar-goltabar@nit.ac.ir
[b] Ph.D., E-mail: Pahlavan@Shahroodut.ac.ir
[c] Ph.D., E-mail: Ghodrati@iust.ac.ir

in the aftermath of an earthquake.

Owing to the high prominence of bridges, it is needed that their damage state be predicted before the occurrence of a ground motion (Domaneschi *et al*. 2017). In this regard, the seismic fragility curves are convenient tools in the evaluation of structural damage through determining the probability of exceeding a specific damage state with respect to building seismic parameters (DesRoches *et al*. 2011, Wang and Ni 2015).

So far, a lot of researches have focused on the deterministic responses of bridges (Zakeri 2013, Banerjee and Shinozuka 2007, Pahlavan *et al.* 2018), while more precise vulnerability assessment can be made using probabilistic methods thru various levels of uncertainty (Mackie *et al.* 2007, Xie *et al*. 2019).

On the other hand, limited inquiry has been performed on the vulnerability of curved concrete box-girder bridges subjected to three-directional earthquake excitations, and thus, the probabilistic investigation of such bridges is of great importance (Falamarz-Sheikhabadi and Zerva 2017, Mangalathu *et al*. 2018, Amjadian and Agrawal 2016).

Nielson (2005), Padgett (2007), Ramanathan (2012), Zakeri (2013) and Mirza Goltabar Roshan *et al*. (2018) carried out widespread researches on the vulnerability and retrofitting of multi-span continuous and simply-supported concrete bridge classes in the central and western United States. However, their studies are dedicated to straight bridges, all asserting that the effect of deck curvature should be considered in the subsequent inspections.

A number of investigations were conducted to assess the vulnerability of bridge inventories over the last decade, which is presented henceforth.

Seo and Linzell (2012) examined the seismic vulnerability of existing horizontally curved steel I-girder bridges in the states of Maryland, New York and Pennsylvania, USA. Their study accounted that for curved bridges under consideration, bearing radial deformations are the most critical components in the bridge vulnerability. Furthermore, it was specified that the number and the length of spans, as well as the radius of curvature, significantly affect fragility curves.

Tondini and Stojadinovic (2012) explored the effect of radius on the seismic behavior of conventional curved box-girder concrete bridges in California. A probabilistic seismic demand model (PSDM) was particularly adopted for a curved bridge of 5 spans with reinforced concrete (RC) box-girder and concrete single-bent columns. The only variable parameter in that research was the horizontal curvature radius of the bridge in plan, disregarding the effects of foundations, abutments, shear keys, bearings, and uncertainties of materials and geometry in the modeling. They considered the column drift as a demand parameter, documenting that the drift increase is more pronounced for curved bridges as compared to straight ones.

Pahlavan *et al*. (2015, 2017) assessed the seismic vulnerability of RC curved bridges via probabilistic approach and developed the fragility curves. The samples were four-span curved bridges with regular column height. Various methods of bridge retrofitting were probabilistically studied in that research. The result determined the effect of different retrofitting methods on the seismic performance of bridges.

Jeon *et al.* (2016) examined the influence of geometric parameters, incorporating column height, abutment skew, and horizontal curve on the seismic response and fragility of curved multi-frame concrete box-girder bridges featuring in-span hinges. To this end, two bridges with integral abutments (two and three frames) with a common configuration of the California bridge class were selected and evaluated for each of the 9 various patterns of abutment skew. Therefore, dynamic time history analyses were performed on the models under a set of ground motion records. In addition, the effect of each geometric parameter was determined on the bridge geometry, and hence, the

fragility curve of each was plotted. Results revealed that most geometric parameters have major impact on the fragility curve of some components, despite the fragility of the whole system. Column height was acknowledged to be the most effective parameter influencing the system fragility, whereas abutment skew and horizontal curvature had negligible effects on the fragility of such bridge class.

To better apprehend the dominance of the two curvature radius and fault proximity, vulnerability of the curved multi-frame concrete box-girder bridges with different radii in the two far- and near-fault events was evaluated. The bridges were modeled in three modes of two-, three-, and four-column bents, commonly constructed in California. The geometric and material property uncertainties were considered in the vulnerability assessment of joint seals, columns, foundations, abutments, bearings, shear keys, deck unseating at abutments, and in-span hinges in the modeling of ground motion.

Based on the guidelines of HAZUS-MH (2011), fragility curves discriminate bridge and structural damages into four slight, moderate, extensive and complete states. Such curves are plotted separately at each damage state for every single ground motion, and are exercised as input parameters in the calculation of structural damage. These curves can be exhibited distinctly for various bridge components, and hence, it is feasible to develop fragility curve of the entire structural system through probabilistic methods, so as to estimate the influence of curvature on the bridge vulnerability.

2. Effects of near-fault and vertical component of ground motion on the bridge response

Following the 1966 Parkfield and the 1971 San Fernando, California, USA, earthquakes, the term near-fault was introduced by Bolt (2004). Although near-fault effects had been known before, the importance of such dispute in designing structures was not well perceived until the ruinous earthquakes of the 1992 Landers, the 1994 Northridge, the 1995 Kobe of Japan, and the 1999 Chi-Chi of Taiwan occurred, causing extensive damage in the near-fault structures (Choi *et al*. 2005, Galal and Ghobarah 2006).

Earthquakes are typically dependent on three factors within the near-fault region. These factors comprise the rupture mechanism, direction of the rupture propagation relative to site, and the permanent displacements due to fault slip. Furthermore, they give rise to two effects, namely, rupture directivity and fling step. For the estimation of earthquakes near the active faults, characteristics of the near-fault earthquakes (rupture directivity and fling step) should then be taken into account. Rupture directivity is distinguished by the two forward and backward directivity effects. When a fault breaks, rupture is generated at a point along the fault and extends toward the beginning, the end, or both directions, depending on the origin of rupture. In this case, forward directivity occurs, provided that fault rupture propagation and fault slip direction are both towards the site. This effect stems from the fact that rupture propagation speed is close to that of shear wave in the rock near the source of earthquake. Generally speaking, the rupture speed in the forward directivity is slightly less than the shear wave speed. In strike-slip mechanism, earthquake energy is compressed along the fault in each rupture. It eventually heads toward the site with a large vibrating pulse accompanied by a shear wave. It then appears in terms of a pulse component (shock) perpendicular to the fault at the beginning of recording. This sort of vibration has essentially a short duration, a high-amplitude special pulse, and a moderate to long period. If the site is near the
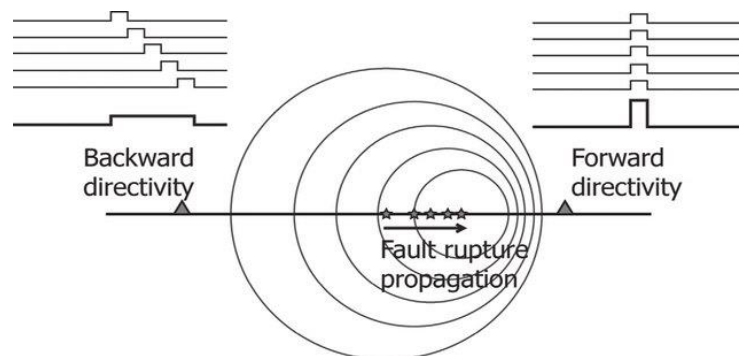
Fig. 1 The effects of forward and backward directivity (Chioccarelli 2010)

epicenter and the rupture propagates away from the site, then backward directivity occurs. Earthquake in the backward directivity mode has a longer duration, multiple pulses with short periods, and a low amplitude, so that earthquake energy is dispersed during the vibration (Stewart *et al*. 2002).

In the near-fault earthquakes, the shear wave subsequent to rupture, propagates toward the site and generates a high-amplitude horizontal pulse-like wave at the beginning of forward-directivity recording, which is perpendicular to the fault (Fig. 1).

Most research efforts conducted so far on the probabilistic vulnerability assessment of curved bridges have considered horizontal excitations, while little research has addressed their vulnerability under tri-directional far- and near-fault excitations. Furthermore, most of the studies considering the vertical component of the earthquake have deterministically reviewed a limited number of records and not addressed the probabilistic seismic damage assessment considering full capacity and demand uncertainties.

Jeon *et al*. (2015) investigated the performance of older highway bridges under vertical components of ground motions. The fragility was defined as the probability of exceeding a specified level of damage for a given intensity measure. This paper considered a typical older two-span single-frame concrete bridge with deck included box-girder system, built in California in 1967. The bridge column was conventionally (non-seismically) designed with insufficient details. For instance, the spacing of transverse reinforcement was too large, and the low shear span-to-section depth ratio could lead to a shear–axial failure. Time history analyses were performed and seismic demand models were then developed. These models were used to derive the component and system fragility curves for the two column shear models under constant and variable axial forces. Comparison of results indicated that shear model with variable axial force increases the probability of failure at severe damage state by about 10% across the entire range of intensity measures, reducing the median intensity measure by more than 15%. This observation revealed that the shear–axial force interaction significantly affects the seismic response of older bridges.

3. Specifications of the considered horizontally-curved RC box-girder bridges

Statistical studies conducted by Yang *et al.* on the US bridge database in California showed that more than 50% of bridges constructed in this state are of multi-span continuous box-girder concrete

Table 1 Considered six bridge radii

Model of Bridge	Radius (m)
R1 (sharp curve)	L/2=66
R2	L=132 m
R3	3L/2=200 m
R4	2L=265 m
R5	3L=400 m
R6 (straight bridge)	10L=1324 m

bridge class. Given the high seismicity of this state, selecting this type of bridge in order to perform the seismic probabilistic studies is of high significance (Yang *et al*. 2009).

According to Ramanathan (2012), if the span number of this bridge class is four or more, the bridge should be fabricated as multi-frames (with in-span hinges). Thereby, this type of bridge has been investigated in the present study, owing to its complicated and unique dynamic behavior.

The bridges under study were constructed during the 1971-1990 era in California with an average length of 132 m. To obtain the effect of curvature radius of the curved box-girder RC bridge on its vulnerability, 6 different radii were considered varying from infinity (straight bridge) to sharp curve radius (Table 1).

4. Analytical models of bridges

Three-dimensional analytical models of bridges are created and analyzed in the Open System for Earthquake Engineering Simulation (OpenSees) platform developed by McKenna *et al*. (2009). Fig. 2 shows the FE models of the bridge considered in this study. Probabilistic seismic demand models are created using the results of nonlinear time history analyses. In this paper, multicolumn bents are considered as the most common type of piers in California. Deck is modeled by using elastic beam-column elements, assuming that it remains elastic during the earthquake according to Caltrans Seismic Design Criteria. Since the longitudinal and transverse responses of bridges are significantly affected by curvature, the spine model with lumped masses along the longitudinal centerline of the bridge may not lead to a real response. Consequently, mass is distributed in the transverse direction along the rigid elements.

The columns are modeled with fiber cross-sections assigned to the nonlinear beam-column elements. Concrete 07 material, provided in OpenSEES, is employed to define the concrete characteristics, where monotonic stress-strain curves for confined and unconfined concrete are characterized according to Chang and Meander's model (1994). Steel bars are modeled using Steel 02 in which Menegotto (1973) steel material model is used, featuring isotropic strain hardening. Rigid links connect the columns to deck in order to transfer the moments and forces. The pile foundations are modeled using translational and rotational springs at the base of each column.

Since this study aims to develop reliable fragility curves for bridge classes across a wide geographic area, different soil profiles from soft to medium and stiff are considered to determine the stiffness of springs according to Ramanathan (2012). It should be noted that multicolumn bents, located on footings, are pinned at the base, and have no rotational stiffness (CALTRANS 2007). These springs are modeled using zero-length elements, as shown in Fig. 2.
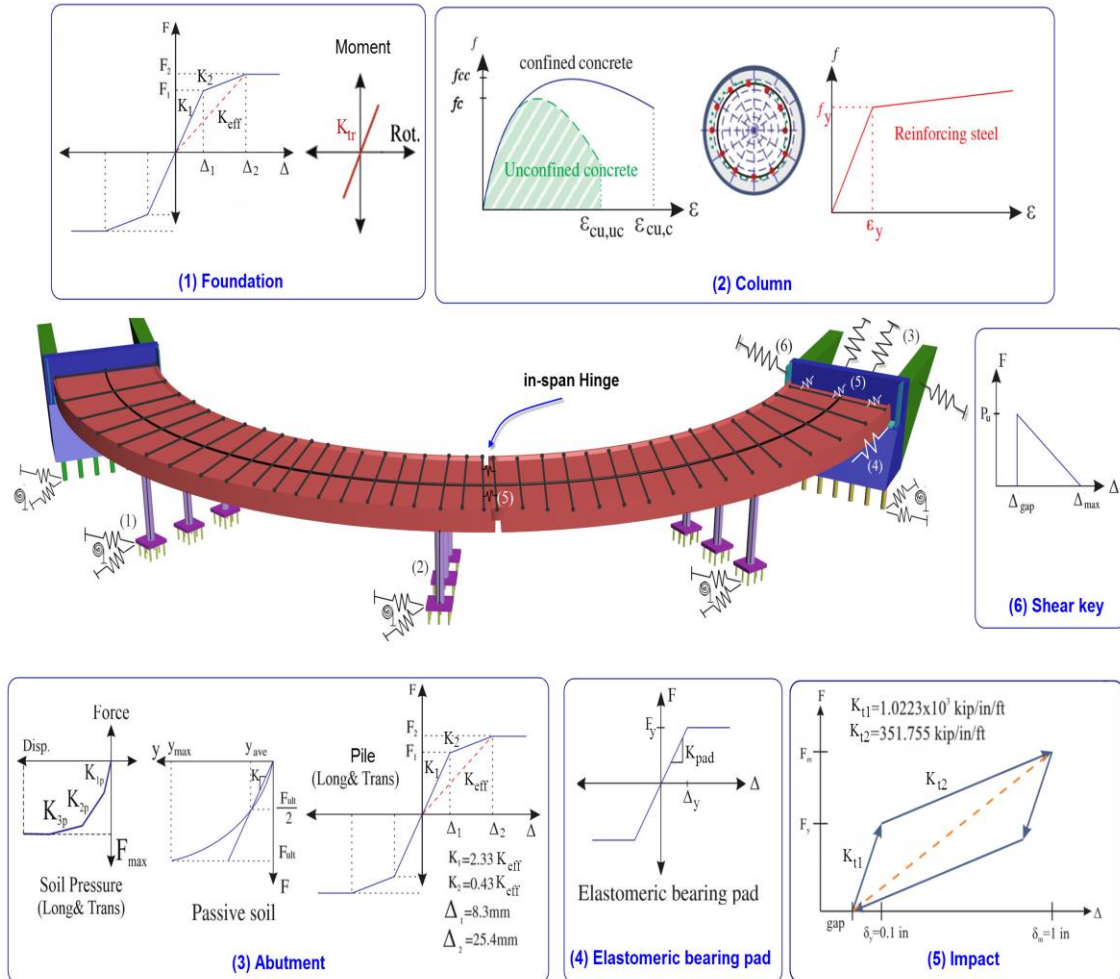
Fig. 2 3D modeling view of bridge along with nonlinear behavior of elements

Large displacements at the abutments have been observed in the past earthquakes. Longitudinal response of the deck can lead to significant soil pressure at the abutment, and thus, increase the impact between deck and abutment back wall in the case of seat type abutments. Nevertheless, response of the abutments in the longitudinal and transverse directions is different. The longitudinal response includes two types of resistance: passive, and active. The backfill soil and the piles provide the passive resistance, whereas active response is provided only by piles. The response of the abutment soil is modeled by zero-length elements based on the nonlinear soil behavior defined by hyperbolic gap material available in OpenSEES, which is established via the model proposed by Shamsabadi *et al*. (2010) and the recommendations of Choi (2002). Longitudinal and transverse stiffness at the abutments are provided by piles. Moreover, Trilinear model presented by Choi (2002) is employed to capture the response of the piles.

In continuous bridge superstructures, movement of deck in the transverse direction is prevented by using exterior shear keys. Therefore, shear keys play a crucial role in the seismic response of

curved multi-span bridges. In this regard, experiments conducted by Megally *et al.* (2001) and Bozorgzadeh *et al*. (2005) showed that these components are prone to have a brittle failure and a sever nonlinear response under earthquakes. The shear key has been modeled in accordance with the experimental study presented by Megally *et al*. (2001). Zero-length elements are employed to depict the response of shear keys based on a nonlinear force-deformation response. Past studies have revealed that in some bridge types including those considered in this study, pounding between adjacent decks at in-span hinges or between decks and abutments under seismic excitations affects the bridge response. Damages such as the crushing of concrete on the deck and the unseating of the deck are among the consequences of the pounding effect in the aftermath of an earthquake. To model the impact between deck and abutment, zero-length elements with a bilinear model have been used according to the approach proposed by Muthukumar (2003) and Muthukumar and DesRoches (2006), normal to the face of the deck are defined. This model is capable of modeling the pounding and the resulting energy loss. Based on the parameters proposed by Nilson (2005), as shown in Fig. 2. The stiffness (K_{t1} and K_{t2}), yield displacement (δ_y), and maximum displacement (δ_m) parameters were considered.

The behavior of elastomeric bearings is specified as the elastic-perfectly plastic material with the concrete-neoprene friction coefficient of 0.40 in compliance with the CALTRANS seismic design criteria (CALTRANS 2004). The shear modulus of elastomeric pads varies from 0.66 to 2.07 MPa, conforming to recommendations presented by Nielson (2005).

Table 2 reports all random variables along with the corresponding distributions. Likewise, the behavior of different bridge components modeled in OpenSEES is expressed in Table 3.

Table 2 Random Variables and Distributions Available in Different Bridge components

Modeling parameter	Probability distribution	Distribution parameter		Units	References
		1	2		
Steel yield strength	Lognormal	λ=29	ζ=0.08	MPa	Ellingwood and Hwang (1985)
Concrete unconfined strength	Normal	μ=34.5	σ=4.3	MPa	Choi (2002)
Elastomeric bearing shear modulus	Uniform	l=551	u=1.723	MPa	Ramanathan (2012)
Coefficient of friction MF|t2fn1	Lognormal	λ=0	ζ=0.1	----	Mander *et al*. (1996) and Dutta (1999)
Piles rotational stiffness	------	0	0	----	CALTRANS (2007)
Piles translational stiffness	Lognormal	λ=7.06	ζ=0.3	kN/mm/pile	CALTRANS (2007)
Abutment passive initial stiffness [a]	Uniform	l=14.5	u=29	kN/mm/m	Shamsabadi et al. (2010)
Damping	Normal	μ=0.045	σ=0.0125	----	Fang *et al*. (1999) and Bavirisetty *et al.* (2000)
Abutment gap	Uniform	l=38.1	u=152	mm	Based upon inventory review
Mass	Uniform	l=1.1	u=1.4	----	Ramanathan (2012)
Loading direction	Uniform	l=0	u=2π	rad	Ramanathan (2012)
Percentage of longitudinal column bars	Uniform	1%	3.7%	----	Ramanathan (2012)
Gap between deck and Abutment	Uniform	0	10	cm	Ramanathan (2012)
Gap between deck and shear key in transverse direction	Uniform	0	4	cm	Ramanathan (2012)

[a] Variables are per unit width of the abutment backwall.

Table 3 Behavior of different bridge components and modeling in OpenSEES

Bridge component or material	Modeled element type and behavior	References
Deck	Elastic beam-column element with calculated section properties	Nielson (2005)
Column	Nonlinear beam-column element with fiber section	Nielson (2005)
Elastomeric bearings	Elastic-perfectly-plastic behavior with steel 01 material applied to zero length element	Nielson (2005)
Impact	Bilinear behavior applied to zero length element	Muthukumar and DesRoches (2006)
Piles	Uniaxial material hysteretic with trilinear behavior	Choi (2002)
Abutment	Hyperbolic gap material with parabolic soil behavior which applied to zero length element	Shamsabadi *et al*. (2010) and Choi (2002)
Shear key	Uniaxial hysteretic behavior applied to zero length element	Megally *et al.* (2001)
Concrete	Concrete 07 material with monotonic stress-strain characteristic	Chang and Mander (1994)
Reinforcing steel bars	Steel 02 material with isotropic strain hardening behavior	Menegotto (1973)

Table 4 Geometric properties of 10 samples of considered curved box-girder concrete bridges using Latin-hypercube technic

Bridge Samples	Number of spans	Number of Columns	Span Length (m)	Deck Width (m)	Column Height (m)
1	4	3	34.28	26.71	4.96
2	4	4	27.47	30.56	6.67
3	4	2	44.01	13.54	3.88
4	4	4	23.97	36.5	5.46
5	4	3	38.4	21.53	4.79
6	4	2	30.77	12.23	6.33
7	4	3	54.93	19.57	4.42
8	4	2	17.16	14.89	5.84
9	4	3	33.36	23.84	5.13
10	4	2	26.63	17.86	7.21

Five various deck radii ranging from 66 to 400 m are selected to investigate the influence of curvature on the vulnerability of four-span curved bridges, apart from the straight model. The length of each span is considered 33 m to represent the typical median span length of such bridge type in California (Ramanathan 2012). In addition, structural attributes are kept constant while radius varies. Fig. 2, illustrates schematic of the considered curved bridge along with the nonlinear behavior of elements.

5. Geometric uncertainties and ground motion characteristics

Given that this class of bridge has a specific status in California, in terms of deck length and width and column height, 10 random sample bridge geometries were selected for each of the 6 radii
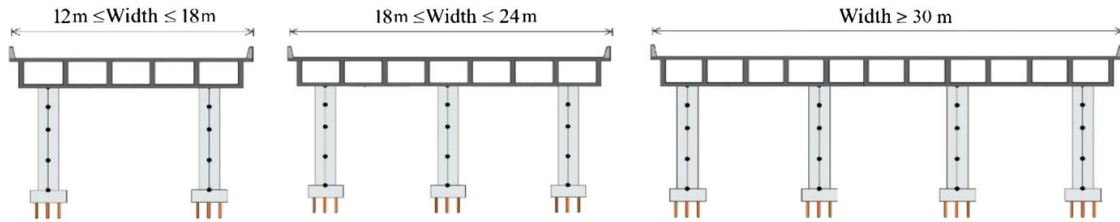
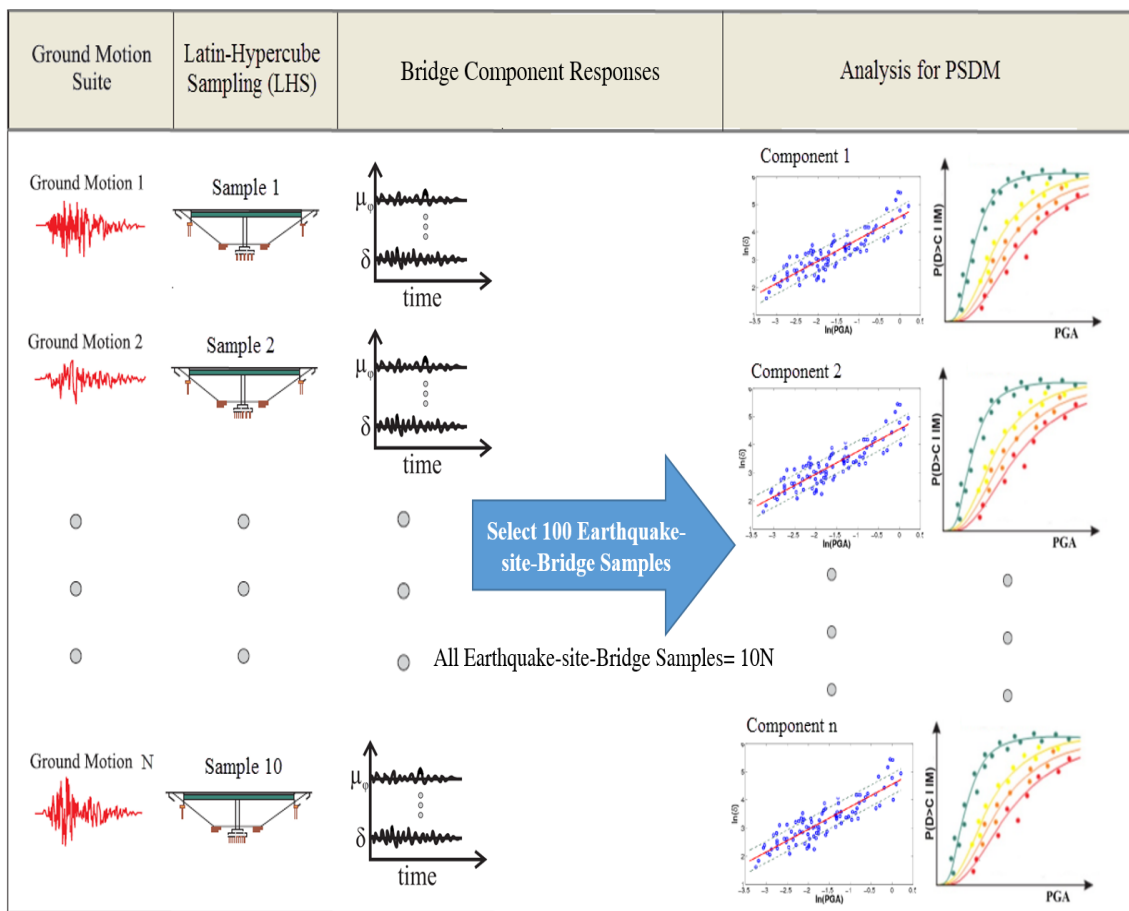Fig. 3 The number of columns per bent with respect to deck width

Fig. 4 Analytical Fragility Curve Generation Using Non-linear Time History Analyses

among all classes of this bridge, adopting a Latin-Hypercube Sampling (LHS) technique (Ayyub and Lai 1989) based on the NBI (2010) database. The attributes are reported in Table 4. These 10 samples represent geometric configurations of the entire statistical population of the curved box-girder bridges in California. For more information on the details of sample specifications, Zakeri's paper (Zakeri *et al*. 2013) should be referred to.

Geometric uncertainty of bridges was measured in creating bridge models with different radii, span lengths, column heights, and deck widths. Regarding the California bridge characteristics and the extensive research carried out by Ramanathan (2012), the number of columns in each bent is different depending on the deck width. According to Fig. 3, the required deck width for each of the 2-, 3-, and 4-column bents are respectively 12 to 18, 18 to 24, and 30 to 40 m.

According to Nielson and Mackie (2009), minimum of 80 records are necessary to reflect the earthquake uncertainty in the probabilistic vulnerability assessment of structures.

This research utilized 120 earthquake records proposed by Baker *et al.* (2011), including 80 near-fault (Set #1A, Set #2) and 40 far-fault records (Set #1B). See Baker *et al.* (2011) for more information on the characteristics of earthquake records.

Each of these records is randomly applied to the considered bridges via LHS technique (Table 4). As can be seen in Fig. 4, from 10 N earthquake- bridge samples, 100 earthquake- bridge samples were selected randomly. N is the number of earthquakes being 80 for near-fault and 40 for far-fault earthquakes. This way, 100 nonlinear time history analyses under the near-fault state, and another 100 analyses for the far-fault state have been performed at each bridge radius. Therefore, 1200 dynamic time history analyses are required for plotting bridge fragility curves for the 6 different radii.

6. Seismic behavior of curved box-girder bridges

To better understand the seismic behavior of bridges with different radii in the far-field and near-field events, a deterministic analysis was executed and hysteretic curves were then compared. Fig. 5, compares the hysteretic curve of a representative bridge with a radius of 265 m for column and bearing components in the two near- and far-fault records.

It can be concluded from Fig. 5 that the energy absorption of bridge components under the far-field ground motion record is much more than that of the near-field record.

7. Modal analysis of bridge

After conducting the modal analysis of the bridges under study, the period values for bridge radii with the geometrical properties of sample 4 are given in Table 5.

As an example, the modal analysis of bridge sample 4 with a radius of 66 m together with its mode shape is provided in Fig 6.

Table 5 Period values for bridge radii

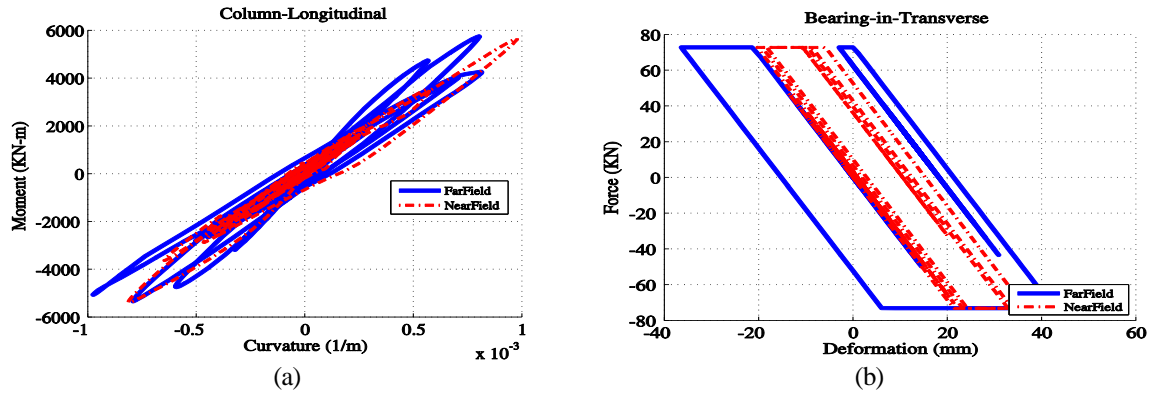| Model of Bridge	First-mode period (T1) (sec)
R1 =66 m	1.49
R2=132 m	3.20
R3=200	4.47
R4=265	5.98
R5=400	8.48

Fig. 5 Hysteresis curve of various bridge components with a radius of 265 m in the two far- and near-fault events, (a) column and (b) bearing
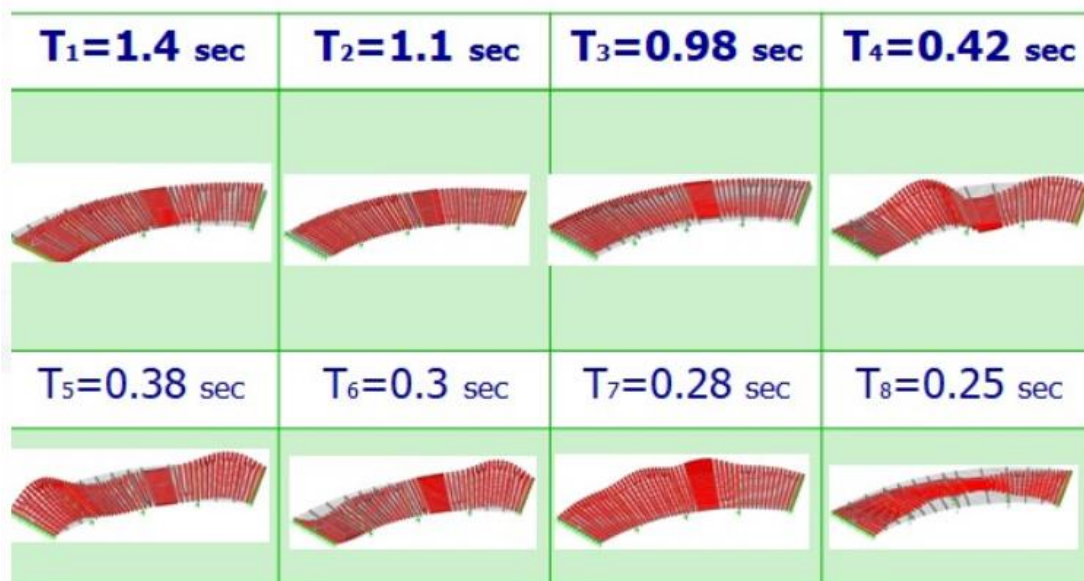

Fig. 6 Modal shape analysis of bridge sample 4 with a radius of 66 m

To better understand the effect of the near-fault records, the predominant periods of the 40 near-fault records selected from Baker *et al.* (2011) used in this study are provided in Table 6. As can be seen, the predominant periods of the earthquake records are significantly different from the periods of the bridges under study, and thus resonance did not occur.

Table 6 Predominant periods of the near-fault records

Record	X	Y	Record	X	Y	Record	X	Y	Record	X	Y
R1	0.56	0.16	R21	0.38	0.28	R41	0.2	0.12	R61	0.14	0.14
R2	0.54	0.62	R22	0.76	0.56	R42	0.24	0.24	R62	0.38	0.38
R3	0.08	0.1	R23	0.08	0.24	R43	0.28	0.28	R63	0.24	0.2
R4	0.06	0.06	R24	0.18	1.76	R44	0.18	0.24	R64	0.9	0.42
R5	0.42	0.74	R25	0.5	0.54	R45	0.3	0.32	R65	0.16	0.16
R6	0.28	0.2	R26	0.22	0.64	R46	0.5	0.16	R66	0.06	0.08
R7	0.74	1.16	R27	0.52	0.68	R47	0.26	0.26	R67	2.94	0.16
R8	0.1	0.2	R28	0.26	0.28	R48	0.26	0.36	R68	0.38	0.16
R9	0.38	0.38	R29	0.54	0.46	R49	0.38	0.2	R69	0.3	0.36
R10	0.32	0.32	R30	0.42	0.22	R50	0.42	0.88	R70	0.28	0.28
R11	0.08	0.18	R31	0.52	0.26	R51	0.22	0.16	R71	0.32	0.44
R12	0.44	0.48	R32	0.18	0.16	R52	0.4	0.32	R72	0.4	0.26
R13	0.3	0.28	R33	0.18	0.54	R53	0.2	0.4	R73	0.14	0.16
R14	0.32	0.32	R34	0.7	1.24	R54	0.18	0.12	R74	0.38	0.34
R15	0.28	0.2	R35	0.36	0.34	R55	0.16	0.12	R75	0.3	0.44
R16	0.32	0.74	R36	0.44	1.56	R56	0.46	0.38	R76	0.38	0.32
R17	0.44	0.62	R37	0.22	0.22	R57	0.4	0.26	R77	0.12	0.12
R18	0.76	1.04	R38	0.22	0.18	R58	0.34	0.44	R78	0.6	0.48
R19	0.24	0.22	R39	0.22	0.32	R59	0.04	0.02	R79	0.6	0.46
R20	0.76	0.62	R40	0.16	0.2	R60	0.16	0.18	R80	0.24	0.2

8. Probabilistic Seismic Demand Models (PSDM)

In order to quantify the vulnerability of various structural components in terms of the rate of earthquake risk, it is plausible for any type of structure, which is susceptible to relative displacement or acceleration, to express the probability of occurrence or exceedance of a specific damage level in terms of an earthquake property such as PGA, PGV, and PGD. According to Nielson and DesRoches (2007a, b), and Padgett (2007), the peak ground acceleration (PGA) is an effective parameter in the seismic demand of structures.

In the probabilistic vulnerability assessment of bridges and the development of fragility curves in this study, PGA has been used as the intensity measure (IM). The component responses in the present study are: column curvature ductility demand (μ), active, passive, and transverse deformations of the abutment, shear key deformation, longitudinal and transverse displacements of the elastomeric bearings at abutments and in-span hinges, deck displacement of abutments, deck displacement of in-span hinges, joint seal displacement of abutments and in-span hinges, as well as foundation displacement and rotation.

Seismic demand models are often dependent on the response of structures as probabilistic models, which can be expressed on an arbitrary scale of earthquake intensity. Based on the model offered by Cornell *et al.* (2002), the relationship between seismic demand and seismic intensity (IM) is expressed in logarithmic form as Eq. (1), (Naseri *et al*. 2017).
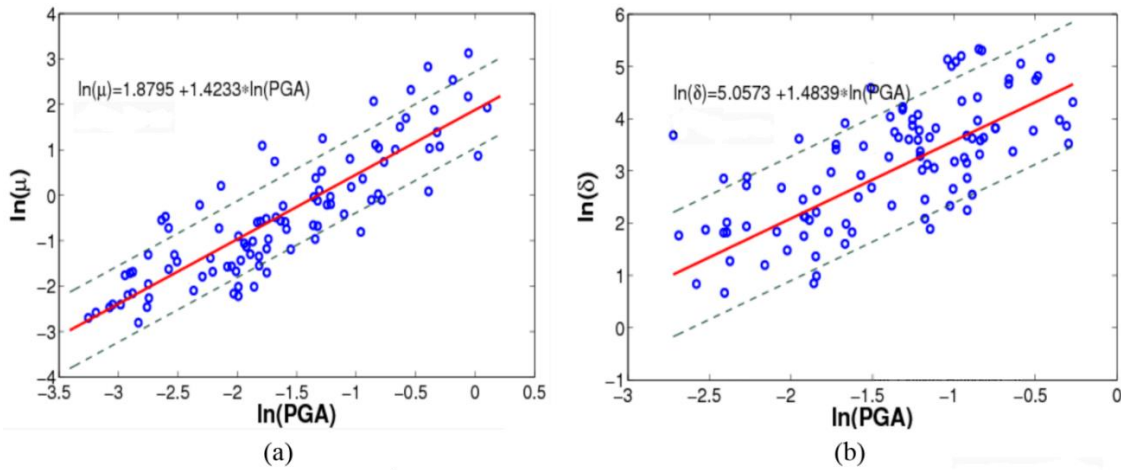
(a)   (b)

Fig. 7 Probabilistic seismic demand model in a representative 132-m radius curved bridge, Column (a), and Abutment (b)

$$\ln(S_d) = \ln(a) + b\ln(IM) \qquad (1)$$

in which a and b are the regression analysis coefficients, and IM is the intensity measure. In this study, a total of 100 nonlinear dynamic analyses were carried out for each of the bridges. The maximum seismic demand for columns and abutments with a radius of 132 m are presented in Fig. 7 (for near-fault). Each point represents an analysis, illustrated in the logarithmic form. The linear regression, obtained from these points, was then plotted. Consequently, S_d can be computed using the equation of the line.

Eq. (2) is used to evaluate the probabilistic vulnerability of bridges and to calculate the fragility curve (Naseri *et al.* 2020).

$$P_f = \Phi\left[\frac{\ln\left(\frac{S_d}{S_c}\right)}{\sqrt{\beta_d^2 + \beta_c^2}}\right] \qquad (2)$$

in which F () is the standard normal cumulative distribution function, P_f is the damage probability, C and D are respectively capacity and demand, S_d and S_c are the median values of demand and capacity determined in view of the damage state, β_d and β_c are respectively logarithmic standard deviations of demand and capacity.

9. Limit state capacity of various bridge components

Having the capacity of each bridge component compared to demand, plus fragility relationships, one is able to calculate the vulnerability of various bridge components as well as the entire bridge system. Regarding Ramanathan (2012), as well as each damage limit state, an uncertainty has to be established for the fragility analysis. A lognormal standard deviation of 0.35 was conservatively suggested for all bridge components at all damage states.

Table 7 Limit state values of the capacity of various bridge components

Component Type	Component name	DC_1		DC_2		DC_3		DC_4		Refrence
		S_c	β_c	S_c	β_c	S_c	β_c	S_c	β_c	
Primary	Column	1	0.35	2	0.35	3.5	0.35	5	0.35	Ramanathan 2012
Primary	Deck unseating (mm)	25	0.35	75	0.35	150	0.35	225	0.35	Fung *et al.* 1971
Secondary	Abut-passive (mm)	75	0.35	250	0.35	N/A	0.35	N/A	0.35	Choi 2002
Secondary	Abut-active (mm)	38	0.35	100	0.35	N/A	0.35	N/A	0.35	Choi 2002
Secondary	Abut-transverse (mm)	25	0.35	100	0.35	N/A	0.35	N/A	0.35	Choi 2002
Secondary	Bearings-longitudinal (mm)	25	0.35	100	0.35	N/A	0.35	N/A	0.35	Ramanathan 2012
Secondary	Bearings-transverse (mm)	25	0.35	100	0.35	N/A	0.35	N/A	0.35	Ramanathan 2012
Secondary	Deck displacement (mm)	100	0.35	300	0.35	N/A	0.35	N/A	0.35	Caltrans 2007
Secondary	Joint seal (mm)	15	0.35	N/A	0.35	N/A	0.35	N/A	0.35	Ramanathan 2012
Secondary	Foundation translation (mm)	25	0.35	100	0.35	N/A	0.35	N/A	0.35	Ramanathan 2012
Secondary	Foundation rotation (rad)	1.5	0.35	6	0.35	N/A	0.35	N/A	0.35	Ramanathan 2012
Secondary	Shear key (mm)	40	0.35	125	0.35	N/A	0.35	N/A	0.35	Megally 2001

Consistent with the recent researches on the fragility analysis of bridges, including Ramanathan (2012) and Zakeri *et al.* (2013), the comprising components of the bridge system are classified into primary and secondary, based on the stability and performance of the bridge subjected to earthquake. Columns and deck unseating are acknowledged as primary components, since the extensive or complete damage of these components may result in bridge instability; while foundation, shear key, bearing, abutment, joint seal, and deck displacement are cited as secondary components, for, damage to them does not substantially disturb the bridge stability.

Capacity of various bridge components, listed in Table 7, have been captured from valid references in the four damage states (slight, moderate, extensive and complete).

Assuming a lognormal distribution, each of the demand and capacity are expressed in terms of two parameters, i.e., median and dispersion. The median and dispersion values of demand are figured based upon the regression analysis of a suit of recorded responses for bridge components, as well as the results of nonlinear dynamic analyses performed in OpenSEES. Likewise, median and dispersion values of capacity are provided for various bridge components, complying with the experimental investigations and observations of the past earthquakes.

Contrary to previous fragility studies of Nielson (2005) or Padgett (2007), in which different bridge components and their contribution in the calculation of seismic fragility of the bridge system were addressed to be of the same significance, the current research distinguishes various bridge components into two primary and secondary levels, on the basis of repair conditions and traffic considerations.

System fragility, based on the common probabilistic seismic demand model of this study, can be determined by recognizing that the need for different bridge components is correlated. If $X = (X_1 X_2, ..., X_n)$ denotes the vector of demands, and X_i is placed on n components of the bridge system, then $Y = \ln(x)$ represents the vector of component demands in the logarithmic variables
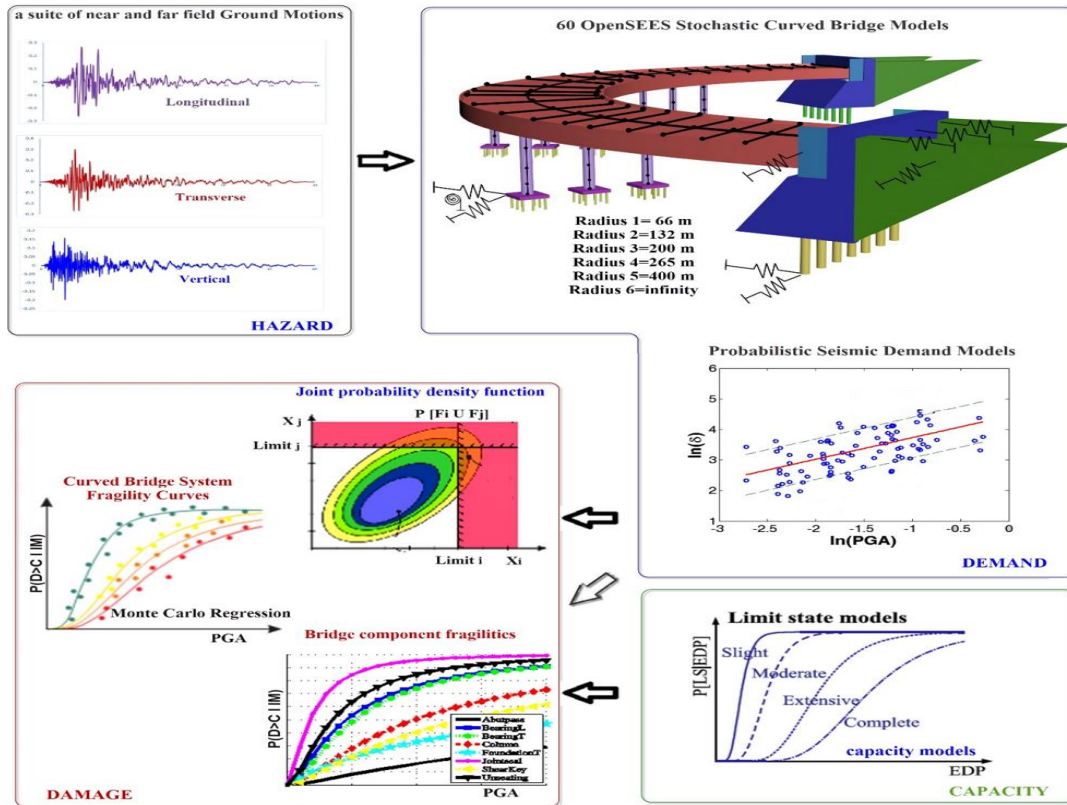
Fig. 8 Implemented seismic fragility assessment framework

space. The common probabilistic seismic demand model is generated in the logarithmic space by creating a median matrix, μ_Y, and the covariance matrix σ_Y. In fact, the covariance matrix considers the correlation coefficients between $\ln(X_i)$. The correlation coefficients between demands of different components of the considered models in the curved RC bridges are obtained via results of time history analysis and the generated covariance matrix. The Monte Carlo simulation approach was employed in order to compare seismic demand with component capacities in the calculation of damage probability of the bridge system.

Probability of demand exceeding capacity is calculated for each component, subjected to a specific earthquake intensity, by creating numerous simulated samples with different demand and capacity values for different components (6 different samples in this study). This process is also reiterated for different earthquake intensities. Afterwards, by performing a regression analysis on the entire data, the median and dispersion values of bridge system fragility are calculated. For a specific level of damage state of the bridge system, the series system hypothesis is then proposed to develop the fragility curves.

Given the series system of considered bridges, bridge seismic fragility is obtained in the four damage states through Eq. (3) (Zakeri 2013)

$$P[DS_j|IM] = \begin{cases} P\left[\bigcup_{i=1}^{N} E_{primary-i}\left(DC_j|IM\right)\right] & , for\ j \geq 3 \\ P\left[\bigcup_{i=1}^{N} E_{primary-i}\left(DC_j|IM\right)\right] + \left[\bigcup_{m=1}^{M} E_{secondary-m}\left(DC_j|IM\right)\right], & for\ j \leq 2 \end{cases} \quad (3)$$

In these equations, M denotes the total number of secondary bridge components, and N indicates the total number of primary bridge components. Moreover, the values of one to four in *j*, correspond to the four damage states from slight to complete. Also, P [DS$_j$ | IM] is the probability of the union of events, where capacity of the ith component of the bridge meets or exceeds the jth damage limit state of that component under a certain earthquake intensity.

The calculations attributed to seismic fragility of the considered bridges were coded in MATLAB software, and fragility curves of the bridge system were then mapped. Fig. 8 schematically expresses how the fragility curves are plotted.

10. Fragility analysis of horizontally-curved box-girder bridge

To investigate the effects of bridge curvature radius and fault proximity (being far or near) on the vulnerability of bridge systems, six different bridge radii were selected in the two far- and near-fault events. Fig. 9 shows the fragility curve of the bridge system with different radii in the far-fault state.
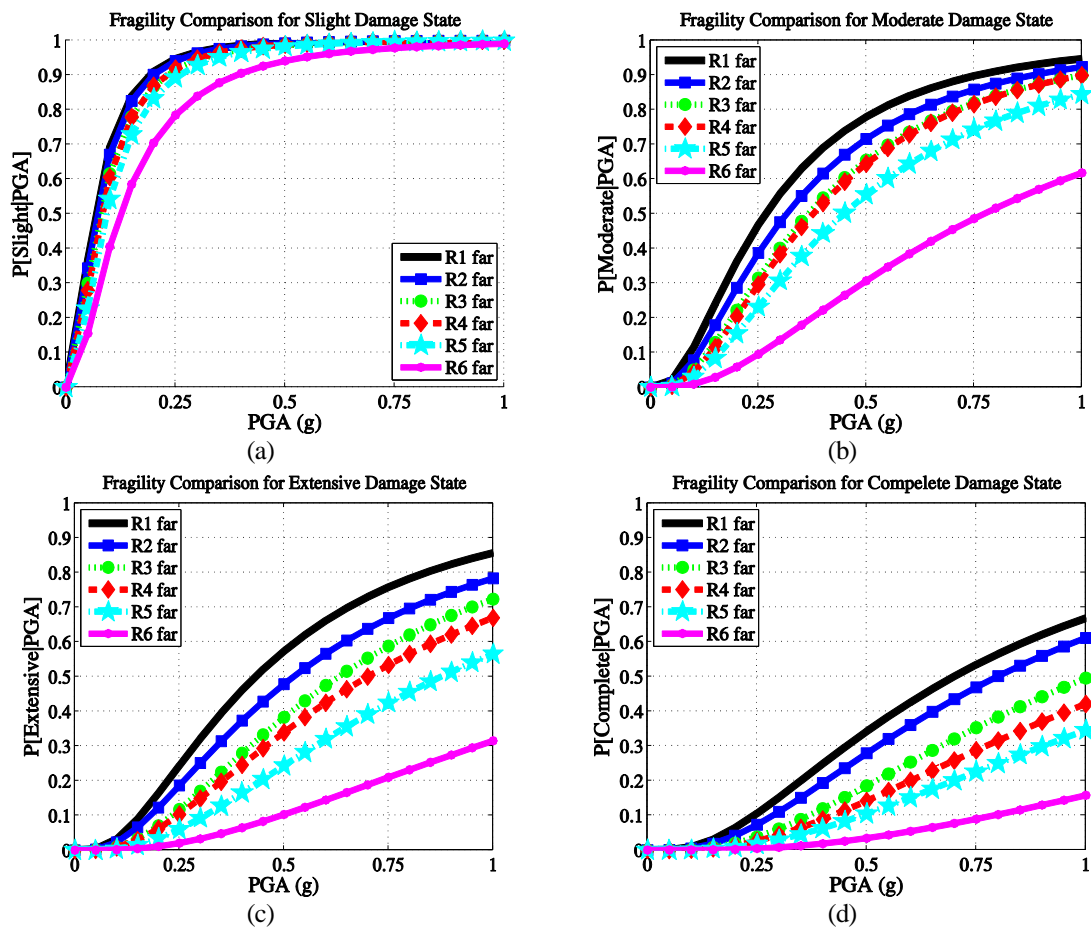

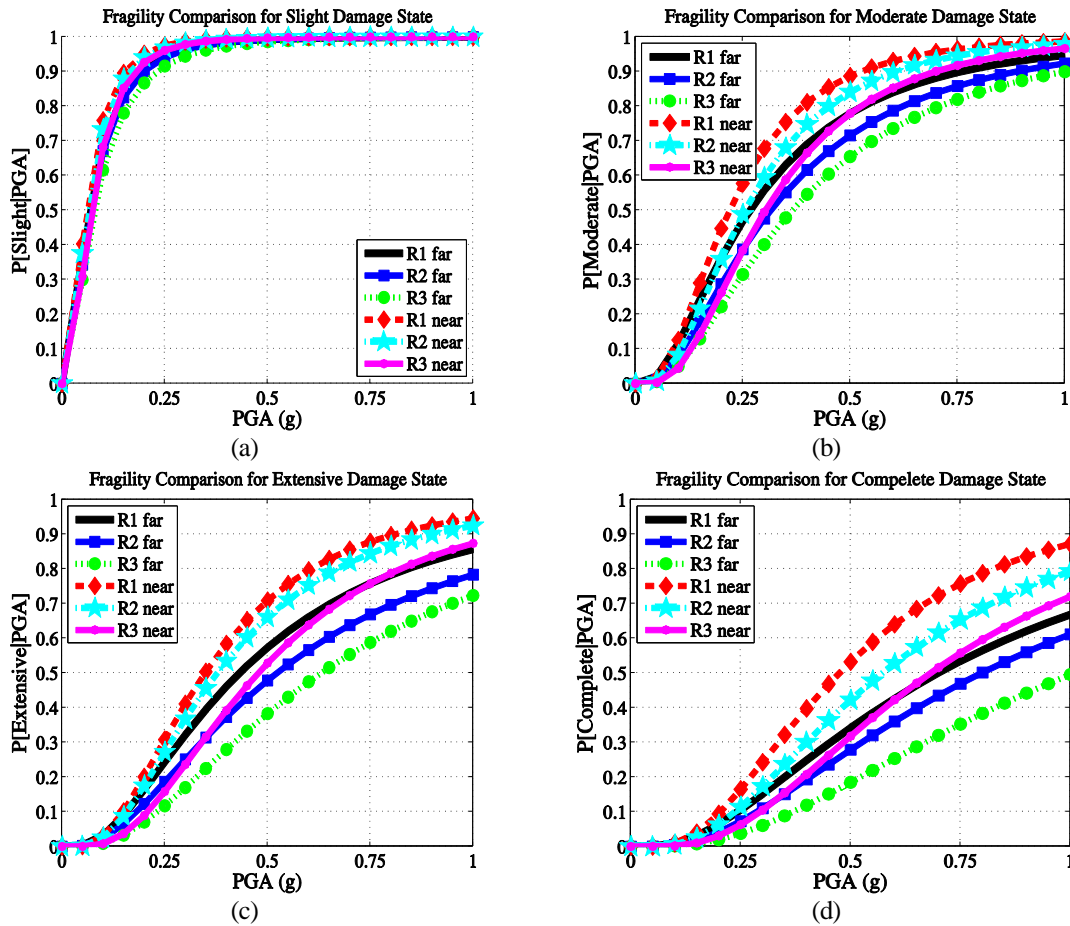Fig. 9 Fragility curves of 6 different bridge radii at four damage states and far-fault event

Fig. 10 Comparison of bridge system fragility curves in the two far- and near-fault events in three radii of R1, R2 and R3

In Figs. 10 and 11, the fragility curves of the bridge system in the two far- and near-fault states are compared in different radii. As shown in the figures, the probability of bridge damage in the near-fault state increases significantly.

Table 8 and Fig. 12, compare the median values of the bridge system fragility in the far- and near-fault events at four damage states.

By comparing the median of bridge system fragility with different radii (66, 132, 200, 265, 400 and 1324 m) in the far- and near-fault events, accounting for the vertical component of earthquake, one can notice that curvature radius and fault proximity are two important parameters in the probabilistic vulnerability assessment of such bridges. For instance, the median of fragility in the complete damage state of the far-fault event varies from 2.328 g for the straight bridge, to 0.698 g for a sharply curved bridge at a radius of 66 m. These values are approximately 1.9 g and 0.47 g for the near-fault event, in order. It is observed that the same trend holds at other damage states.
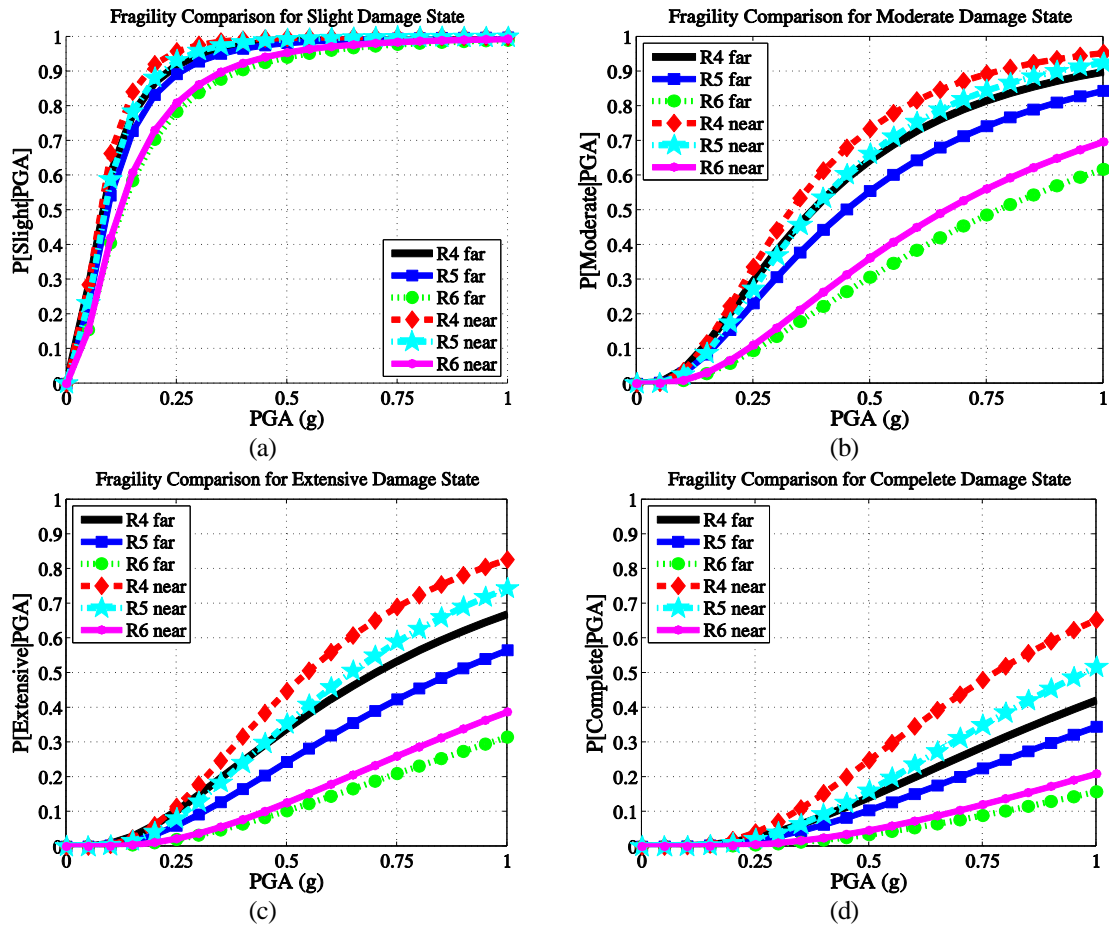
Fig. 11 Comparison of bridge system fragility curves in the two far- and near-fault events in three radii of R4, R5 and R6

Variation trend of the median fragility in different radii in far- and near-fault events is shown in Fig. 13. As it is witnessed, the median fragility increases with increasing radius, indicating that the vulnerability of bridge system is reduced. In extensive and complete damage states of the straight bridge, gradient of the median fragility slope noticeably increases, and thus, the bridge vulnerability further decreases.

The seismic fragility curves of various components are displayed in Fig. 14 for one of the six bridge samples with a radius of 66 m. Similarly, the effect of far- and near-fault events on the median fragility of various bridge components at slight damage state is presented in Fig. 15.

As it is noted in Figs. 14 and 15, joint seal is the most vulnerable component of the bridge at slight damage state. It is followed by deck unseating, which has the highest probability of damage in an earthquake with a given PGA. At this damage level, the passive displacement component of abutment has the least probability of damage.

Table 8 Median fragility Values of bridge system in the far- and near-fault events at four damage states

| Radius		Slight		Moderate		Extensive		Complete	
		med	dis	med	dis	med	dis	med	dis
R1=66 m	Near Field	0.060	0.730	0.219	0.683	0.348	0.659	0.474	0.656
	Far Field	0.066	0.822	0.266	0.817	0.432	0.788	0.698	0.821
R2=132 m	Near Field	0.063	0.739	0.255	0.674	0.377	0.678	0.572	0.685
	Far Field	0.070	0.819	0.315	0.808	0.522	0.827	0.798	0.797
R3=200 m	Near Field	0.071	0.712	0.303	0.652	0.477	0.646	0.682	0.655
	Far Field	0.078	0.846	0.365	0.787	0.630	0.778	1.009	0.783
R4=265 m	Near Field	0.074	0.700	0.330	0.660	0.544	0.646	0.775	0.646
	Far Field	0.080	0.812	0.377	0.765	0.700	0.813	1.170	0.792
R5=400 m	Near Field	0.085	0.723	0.377	0.678	0.644	0.674	0.972	0.669
	Far Field	0.092	0.808	0.448	0.793	0.875	0.806	1.379	0.807
R6=1324 m	Near Field	0.119	0.850	0.662	0.798	1.258	0.805	1.901	0.794
	Far Field	0.124	0.893	0.772	0.861	1.529	0.883	2.328	0.842
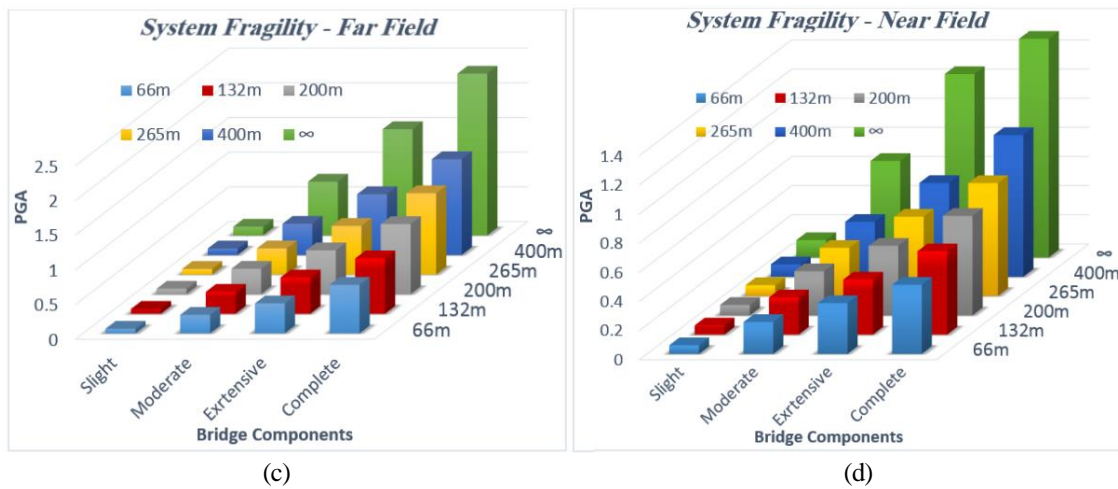
Fig. 12 Plot of the median fragility of bridge system in the far and near-fault states at four damage states in 6 different radii

Given the past earthquakes, the column failure and deck unseating from the abutment were reported to have the greatest damage (Ramanathan 2012, Zakeri *et al.* 2013, Fung *et al.* 1971). Similarly, in the present study, the greatest damage in the moderate, extensive and complete states was associated with the failure of column component and then the unseating of deck component. Accordingly, the median values of fragility of these two components at extensive and complete states in the two far-and near-fault events are compared in Fig. 16. As it is perceived, deck curvature of the curved bridge has a significant effect on the fragility of these two components. Additionally, by decreasing deck curvature radius of the curved RC bridge at extensive and complete damage states,
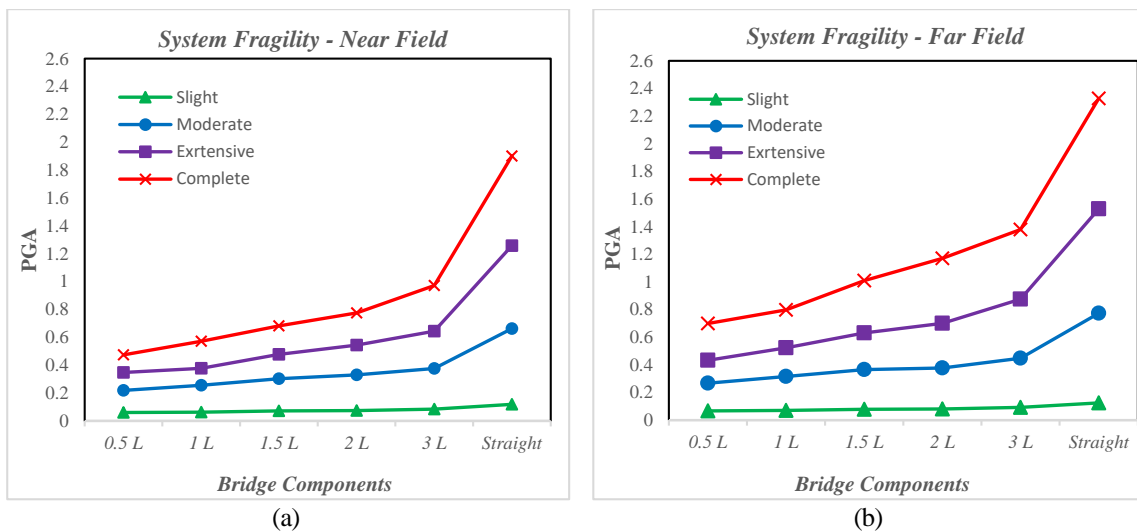
Fig. 13 Variation trend of the median fragility of bridge system in different radii. (a) Near-fault and (b) Far-fault
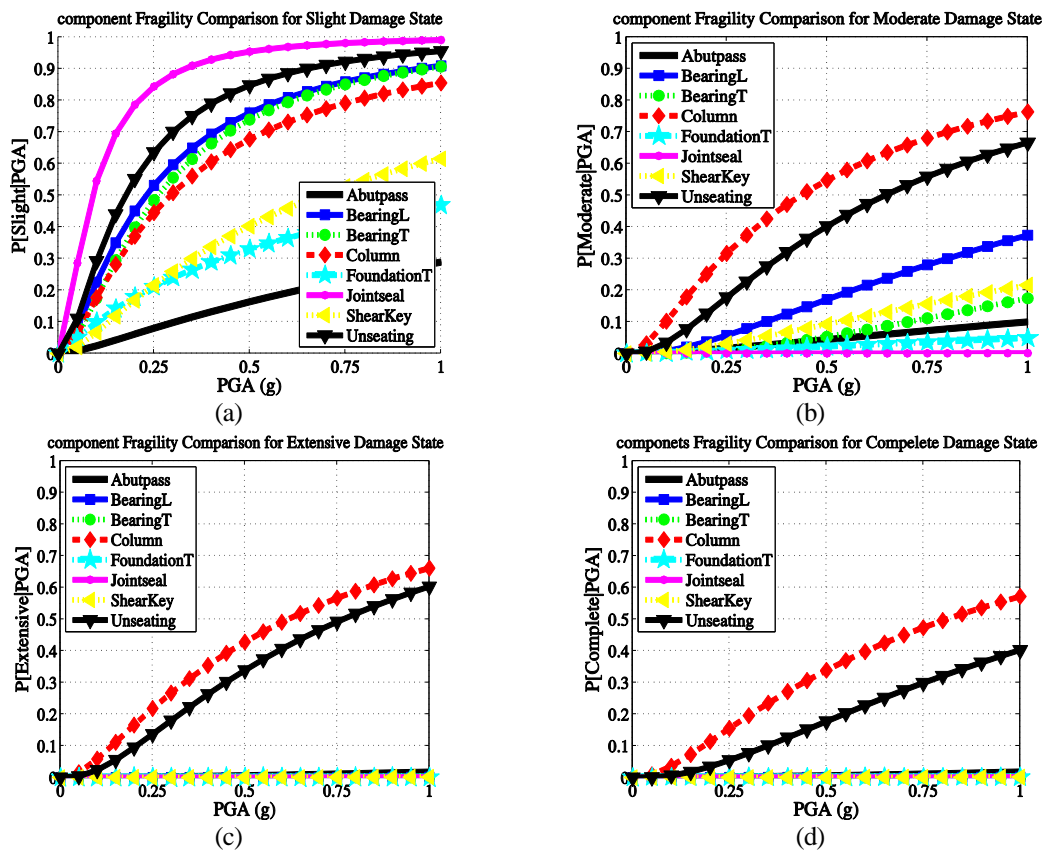

Fig. 14 Fragility curve of various bridge components with a radius of 66 m in the far-fault event
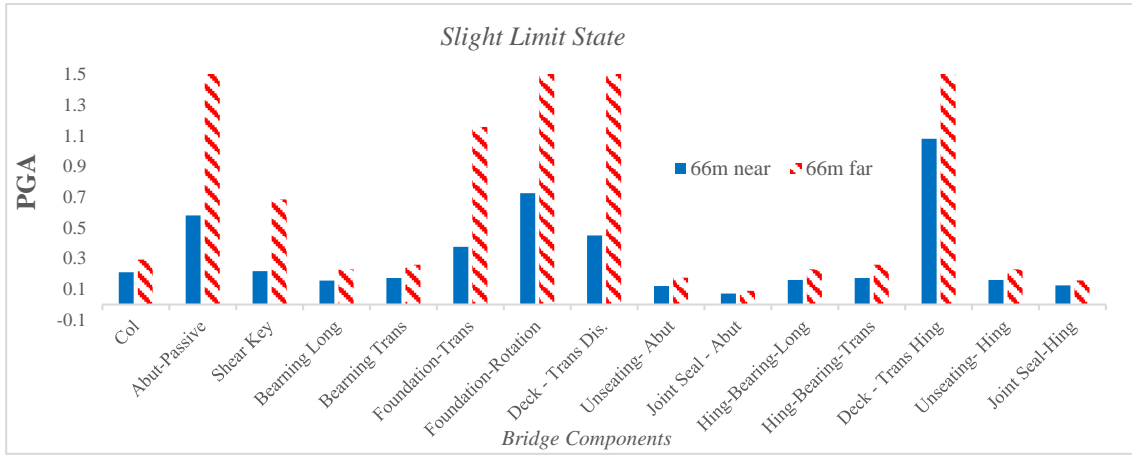
Fig. 15 Median fragility values of various bridge components with a radius of 66 m in the far- and near-fault events at slight damage state
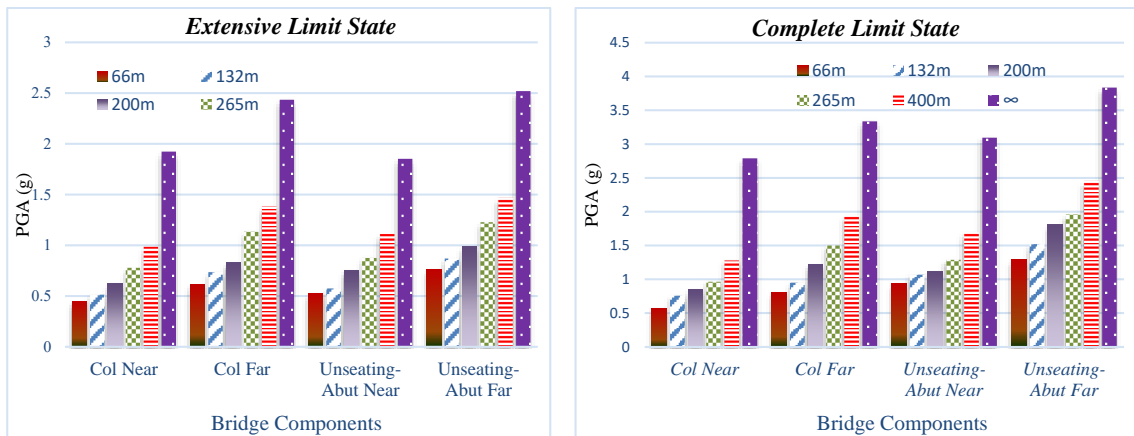

Fig. 16 Median values of fragility of column and deck unseating components in the far- and near-fault events at extensive and complete damage states

the probability of column failure and deck unseating increases. On account of coupling (interaction) of the seismic responses of bridge in longitudinal and transverse directions and the increase of demand, transverse displacement of deck will be larger in curved bridges with lower radii.

As shown in Fig. 16, columns in curved bridges are the most vulnerable components at extensive and complete damage states. This is why the most of bridge seismic vulnerability regulations around the world, including HAZUS-MH, recommend column damage as the only criterion for bridge failure. However, it was proved that such assumption is incorrect, and the contribution of different components of a bridge in the probabilistic seismic assessment will lead to higher fragility. As an example, the median value of fragility of a column in a curved bridge with radius 66 m in the near-fault event is equal to 0.57 g, while this value is 0.47 g for the bridge system in the near-fault event.

Table 9 Median of fragility ratio of bridge system, far-fault to near-fault state in the 6 bridge radii

Radius	Median Ratio	Slight	Moderate	Extensive	Complete	Average
R1=66 m	Far/Near	1.108	1.217	1.241	1.473	1.260
R2=132 m	Far/Near	1.102	1.235	1.385	1.395	1.279
R3=200 m	Far/Near	1.094	1.207	1.321	1.480	1.276
R4=265 m	Far/Near	1.081	1.140	1.286	1.510	1.254
R5=400 m	Far/Near	1.079	1.189	1.360	1.419	1.262
R6=1324 m	Far/Near	1.043	1.166	1.215	1.225	1.162
	Average	1.08	1.19	1.30	1.42	1.25

Table 10 Results comparison of straight bridge by HAZUS (2011) versus those of curved bridge considered in this study

		Slight		Moderate		Extensive		Complete	
		med	dis	med	dis	med	dis	med	dis
HWB23 HAZUS		0.91	0.6	0.91	0.6	1.05	0.6	1.38	0.6
R1=$\frac{L}{2}$ =66 m	Near	0.0598	0.73	0.2189	0.683	0.3479	0.659	0.4742	0.656
	Far	0.0663	0.822	0.2664	0.817	0.4317	0.788	0.6984	0.821

This confirms that the contribution of all bridge components has to be accounted for in a proper probabilistic seismic assessment.

It is discerned, respecting the figures, the median values of column fragility in the far-fault event ranges from 2.43 g for the straight bridge, to 0.617 g for a sharply curved bridge with a radius of 66 m at the extensive damage state. The corresponding values are respectively 1.92 g and 0.45 g in the near-fault event.

Likewise, these values are in the range of 3.36 g to 0.81 g, respectively for the straight and sharply curved bridges at the complete damage state and the far-fault event. The corresponding values are 2.78 g and 0.57 g in the near-fault event, in order.

Table 9 demonstrates the median of fragility ratio of the bridge system in the far-to-near-fault event for various radii. As it is observed, median of fragility in the far-fault event approximately increases by 1.04 to 1.51 times greater than the near-fault event, implying a drastic escalation in the vulnerability of near-fault event. Generally, with increasing damage level from the slight to complete state, median of fragility ratio in the far-to-near-fault event increases. The average value of this ratio in the slight, moderate, extensive and complete damage states is respectively 1.08, 1.19, 1.3 and 1.42.

11. Comparing median values of fragility with HAZUS-MH regulation

The HWB23 bridges are representatives of straight multi-span RC box-girder bridges in the HAZUS-MH regulation. Table 10 compares the fragility values of a curved bridge with a radius of 66 m to those of corresponding values for straight bridges recommended by the US vulnerability regulation, i.e., HAZUS-MH.

The apparent discrepancy in values is justified by two main reasons: firstly, in the seismic vulnerability assessment of bridges through HAZUS-MH, damage to column is considered to be the only damage criterion of RC bridges in the fragility analysis. Secondly, the effects of bridge deck curvature and vertical component of earthquake are not included in the calculation of seismic vulnerability. On the other hand, HAZUS-MH reports the results dispersion as to be 0.6 at all damage levels; while this research has obtained a unique dispersion number at each damage level, indicative of its higher accuracy compared to previous researches.

12. Conclusions

In the present research, three-dimensional probabilistic seismic vulnerability of the curved multi-frame concrete box-girder bridges (having in-span hinges) was delved in the two far- and near-fault events subjected to three-directional ground motion excitations (considering the vertical component of earthquake). Bridge models were analyzed in 6 different radii (66, 132, 200, 265, 400 and 1324 m) subjected to 120 earthquake records, proposed by Baker *et al.* (2011), including 80 near-fault and 40 far-fault records by taking into account all demand (14 uncertainties inherent of bridge, along with the earthquake uncertainty) and capacity uncertainties.

Of all bridges of this class, a total of 10 completely random geometries, representing the geometric status of the entire statistical population of curved box-girder bridges in California, were selected for each of the six bridge radii using the Latin-Hypercube Sampling technique.

Having performed 1200 nonlinear dynamic analyses (ten different geometries and six deck radii subjected to earthquake records in the far- and near-fault events), the fragility curve of each bridge component was plotted, and the effect of curvature on the vulnerability of various bridge components, including joint seals, columns, abutments, foundations, elastomeric bearings, shear keys, and unseating of the deck was investigated. Therefore, by comparing seismic demand with the capacity of components through Monte Carlo simulation strategy, damage probability of the bridge system was estimated.

Results of fragility curves of bridge components revealed that, at slight damage state, the abutment joint seal has the highest vulnerability; while at other damage states, columns and then deck unseating are the most vulnerable components in curved bridges. Comparison of the median values of fragility for bridge systems at different radii in the two far- and near-fault events indicated that the effects of curvature and fault proximity are the two important factors, playing a significant role in the seismic vulnerability of such bridges.

Furthermore, the median of system fragility ratio of the far-to-near-fault event was investigated. It was comprehended that the ratio in the far-fault event approximately increases by 1.04 to 1.51 times greater than that of the near-fault event, implying a severe escalation in the vulnerability of near-fault event. Generally, the median of fragility ratio in the far-to-near-fault event increases with increasing the damage level from slight to complete. The average value of this ratio in the slight, moderate, extensive and complete damage states is respectively 1.08, 1.19, 1.3 and 1.42.

Regulations for the seismic assessment of bridges such as HAZUS-MH do not consider the effects of near-field earthquake records on the seismic fragility assessment of curved bridges. The results of this study can serve the future regional risk assessments, regarding the importance of either including or excluding the near-field effects on the seismic performance of horizontally curved bridges.

Acknowledgements

References

Amjadian, M. and Agrawal, A.K. (2016), "Rigid-body motion of horizontally curved bridges subjected to earthquake-induced pounding", *J. Bridge Eng.*, **21**(12), 04016090.

Ayyub, B.M. and Lai, K.L. (1989). Structural reliability assessment using latin hypercube sampling, In Structural Safety and Reliability.

Baker, J.W., Lin, T., Shahi, S.K. and Jayaram, N. (2011), New ground motion selection procedures and selected motions for the PEER transportation research program. Pacific Earthquake Engineering Research Center, University of California, Berkeley, Berkeley, CA, PEER Report (2011/3).

Banerjee, S. and Shinozuka, M. (2007), "Nonlinear static procedure for seismic vulnerability assessment of bridges", *Comput.-Aided Civil Infrastruct. Eng.*, **22**(4), 293-305.

Bavirisetty, R., Vinayagamoorthy, M. and Duan, L. (2000), Dynamic analysis. Bridge engineering handbook, (Eds., W.F. Chen and L. Duan), CRC Press, Boca Raton, FL.

Bolt, B.A. (2004), "Seismic input motions for nonlinear structural analysis", *ISET J. Earthq. Technol.*, **41**(2), 223-232.

Bozorgzadeh, A., Megally, S., Restrepo, J. and Ashford, S. (2005), "Seismic response and capacity evaluation of sacrificial exterior shear keys of bridge abutments", Dept. of Structural Engineering, Univ. of California, San Diego

CALTRANS (2004), Seismic Design Criteria. (Version 1.3), California Department of Transportation, Sacramento, California.

CALTRANS. (2007), Reinforced concrete bridge capacity assessment training manual. Structure Maintenance and Investigations Rep., Sacramento, CA.

Chang, G. and Mander, J.B. (1994), Seismic energy based fatigue damage analysis of bridge columns: part 1-evaluation of seismic capacity.

Chioccarelli, E. (2010), Design earthquakes for PBEE in far-field and near-source conditions (Doctoral dissertation, PhD Thesis, Dipartimento di ingegneria Strutturale, Università degli Studi di Napoli Federico II, Italy, available at: http://www. dist. unina. it/doc/tesidott/PhD2010. Chioccarelli. pdf).

Choi, E. (2002), Seismic analysis and retrofit of mid-America bridges (Doctoral dissertation, School of Civil and Environmental Engineering, Georgia Institute of Technology).

Choi, I., Kim, M.K., Choun, Y.S. and Seo, J.M. (2005), "Shaking table test of steel frame structures subjected to scenario earthquakes", *Nuclear Eng. Technol.*, **37**(2), 191-200.

Cornell, C.A., Jalayer, F., Hamburger, R.O. and Foutch, D.A. (2002), "Probabilistic basis for 2000 SAC federal emergency management agency steel moment frame guidelines", *J. Struct. Eng.*, **128**(4), 526-533.

DesRoches, R., Comerio, M., Eberhard, M., Mooney, W. and Rix, G.J. (2011), "Overview of the 2010 Haiti earthquake", *Earthq. Spectra*, **27**(1), 1-21.

Domaneschi, M., Sigurdardottir, D. and Glisic, B. (2017), "Damage detection on output-only monitoring of dynamic curvature in composite decks", *Struct. Monit. Maint.*, **4**(1), 1-15.

Dutta, A. (1999), On energy based seismic analysis and design of highway bridges (Doctoral dissertation, State University of New York at Buffalo).

Ellingwood, B. and Hwang, H. (1985), "Probabilistic descriptions of resistance of safety-related structures in nuclear plants", *Nuclear Eng. Design*, **88**(2), 169-178.

Falamarz-Sheikhabadi, M.R. and Zerva, A. (2017), "Analytical seismic assessment of a tall long-span curved reinforced-concrete bridge. Part I: numerical modeling and input excitation", *J. Earthq. Eng.*, **21**(8), 1305-1334.

Fang, J., Li, Q., Jeary, A. and Liu, D. (1999), "Damping of tall buildings: Its evaluation and probabilistic characteristics", *Struct. Des. Tall Build.*, **8**(2), 145-153.

Fung, G., LeBeau, R., Klein, E., Belvedere, J. and Goldschmidt, A. (1971), Field investigation of bridge damage in the

San Fernando earthquake. Bridge Department, Division of Highways, California Department of Transportation, Sacramento, California. Preliminary Report.

Galal, K. and Ghobarah, A. (2006), "Effect of near-fault earthquakes on North American nuclear design spectra", *Nuclear Eng. Design*, **236**(18), 1928-1936.

HAZUS-MH (2011), Multi-Hazard Loss Estimation Methodology: Earthquake Model HAZUS-MH MR5 Technical Manual, Federal Emergency Management Agency, Washington DC.

Jeon, J.S., DesRoches, R., Kim, T. and Choi, E. (2016), "Geometric parameters affecting seismic fragilities of curved multi-frame concrete box-girder bridges with integral abutments", *Eng. Struct.*, **122**, 121-143.

Jeon, J.S., Shafieezadeh, A., Lee, D.H., Choi, E. and DesRoches, R. (2015), "Damage assessment of older highway bridges subjected to three-dimensional ground motions: characterization of shear–axial force interaction on seismic fragilities", *Eng. Struct.*, **87**, 47-57.

Mackie, K.R., Wong, J.M. and Stojadinovic, B. (2007), Integrated probabilistic performance-based evaluation of benchmark reinforced concrete bridges (PEER Report 2007/09). Berkeley, CA: Pacific Earthquake Engineering Research Center, University of California.

Mander, J.B., Kim, D.K., Chen, S.S. and Premus, G.J. (1996), Response of steel bridge bearings to the reversed cyclic loading. Rep. No. NCEER 96-0014, NCEER.

Mangalathu, S., Choi, E., Park, H.C. and Jeon, J.S. (2018), "Probabilistic Seismic Vulnerability Assessment of Tall Horizontally Curved Concrete Bridges in California", *J. Perform. Constr. Fac.*, **32**(6), 04018080.

McKenna, F., Scott, M.H. and Fenves, G.L. (2009), "Nonlinear finite-element analysis software architecture using object composition", *J. Comput. Civil Eng.*, **24**(1), 95-107.

Megally, S.H., Silva, P.F. and Seible, F. (2001), Seismic response of sacrificial shear keys in bridge abutments, Report No. SSRP-2001/23, Department of Structural Engineering, University of California, San Diego, (2001).

Menegotto, M. (1973), "Method of analysis for cyclically loaded RC plane frames including changes in geometry and non-elastic behavior of elements under combined normal force and bending", *Proceedings of the IABSE symposium on resistance and ultimate deformability of structures acted on by well defined repeated loads.*

Mirza Goltabar Roshan, A, Naseri, A. and Pati, Y.M. (2018), "Probabilistic evaluation of seismic vulnerability of multi-span bridges in northern of Iran", *J. Struct. Constr. Eng.*, **5**(1), 36-54 (in persian).

Muthukumar, S. (2003), A contact element approach with hysteresis damping for the analysis and design of pounding in bridges (Doctoral dissertation, Georgia Institute of Technology).

Muthukumar, S. and DesRoches, R. (2006), "A Hertz contact model with non-linear damping for pounding simulation", *Earthq. Eng. Struct. D.*, **35**(7), 811-828.

Naseri, A., Mirzagoltabar roshan, A., Pahlavan, H. and Ghodrati Amiri, G. (2020), "Probabilistic seismic assessment of RC box-girder bridges retrofitted with FRP and steel jacketing", *Coupled Syst. Mech.*, **9**(4), 359.

Naseri, A., Pahlavan, H. and Ghodrati Amiri, G. (2017), "Probabilistic seismic assessment of RC frame structures in North of Iran using fragility curves", *J. Struct. Constr. Eng.*, **4**(4), 58-78. doi: 10.22065/jsce.2017.78827.1095.

NBI. (2010), (National Bridge Inventory), National Bridge inventory data, U.S. Dept. of Transportation, Federal Highway Administration, Washington, DC.

Nielson, B.G. (2005), Analytical fragility curves for highway bridges in moderate seismic zones (Doctoral dissertation, Georgia Institute of Technology).

Nielson, B.G. and DesRoches, R. (2007a), "Analytical seismic fragility curves for typical bridges in the central and southeastern United States", *Earthq. Spectra*, **23**(3), 615-633.

Nielson, B.G. and DesRoches, R. (2007b), "Seismic fragility methodology for highway bridges using a component level approach", *Earthq. Eng. Struct. D.*, **36**(6), 823-839.

Nielson, B.G. and Mackie, K.R. (2009), "Tracking uncertainties from component level to system level fragility analyses through simulation", *Proceedings of the 10th Technical Council on Lifeline Earthquake Engineering (TCLEE) Int. Conf. on Structural Safety and Reliability. Reston*, VA: ASCE.

Padgett, J.E. (2007), Seismic vulnerability assessment of retrofitted bridges using probabilistic methods (Georgia Institute of Technology.

Pahlavan, H., Naseri, A., Rafiei, S. and Baghery, H. (2018), Seismic Vulnerability Assessment of Horizontally Curved Multi frame RC Box-Girder Bridges Considering the Effect of Column Heights and Span Numbers.

Pahlavan, H., Zakeri, B. and Ghodrati Amiri, G. (2017), "Probabilistic Performance Assessment of Retrofitted

Horizontally Curved Multi-Frame RC Box-Girder Bridges", *J. Earthq.Tsunami*, **11**(4), p 1750010.

Pahlavan, H., Zakeri, B., Amiri, G.G. and Shaianfar, M. (2015), "Probabilistic vulnerability assessment of horizontally curved multiframe RC box-girder highway bridges", *J. Perform. Constr. Fac.*, **30**(3), p 04015038.

Ramanathan, K.N. (2012), Next generation seismic fragility curves for California bridges incorporating the evolution in seismic design philosophy (Doctoral dissertation, Georgia Institute of Technology).

Seo, J. and Linzell, D.G. (2012), "Horizontally curved steel bridge seismic vulnerability assessment", *Eng. Struct.*, **34**, 21-32.

Shamsabadi, A., Khalili-Tehrani, P., Stewart, J.P. and Taciroglu, E. (2010), "Validated simulation models for lateral response of bridge abutments with typical backfills", *J. Bridge Eng.*, **15**(3), 302-311.

Stewart, J.P., Chiou, S.J., Bray, J.D., Graves, R.W., Somerville, P.G. and Abrahamson, N.A. (2002), "Ground motion evaluation procedures for performance-based design", *Soil Dynam. Earthq. Eng.*, **22**(9-12), 765-772.

Tondini, N. and Stojadinovic, B. (2012), "Probabilistic seismic demand model for curved reinforced concrete bridges", *Bull. Earthq. Eng.*, **10**(5), 1455-1479.

Wang, J.Y. and Ni, Y.Q. (2015), "Refinement of damage identification capability of neural network techniques in application to a suspension bridge", *Struct. Monit. Maint.*, **2**(1), 77-93.

Xie, Y., Zhang, J., DesRoches, R. and Padgett, J.E. (2019), "Seismic fragilities of single-column highway bridges with rocking column-footing", *Earthq. Eng. Struct. D.*, **48**(7), 843-864.

Yang, C.S., DesRoches, R. and Padgett, J.E. (2009), "Analytical fragility models for box girder bridges with and without protective systems", *Proceedings of the Structures Congress 2009*: Don't Mess with Structural Engineers: Expanding Our Role (pp. 1-10).

Zakeri, B. (2013), Seismmic Vulnerability Assessment of Retrofitted Skewed Concrete Bridges Using Probabilistic Methods (PhD thesis) Iran University of Science and Technology.

Zakeri, B., Padgett, J.E. and Ghodrati Amiri, G. (2013), "Fragility assessment for seismically retrofitted skewed reinforced concrete box girder bridges", *J. Perform. Constr. Fac.*, **29**(2), p 04014043.

JK